Analysis of a Membrane-Type Polymeric-Based Tactile Sensor for Biomedical and Medical Robotic Applications

Javad Dargahi[1*] and Siamak Najarian[2**]

[1]Mechanical and Industrial Engineering, CONCAVE Research Centre, CR-200,
Concordia University, Department of Mechanical and Industrial Engineering,
1445 de Maisonneuve Blvd. West, Montreal, Quebec, Canada H3G 1M8
[2]Biomedical Engineering, Faculty of Biomedical Engineering, Biomechanics Department,
Amirkabir University of Technology, Tehran, Iran

   In this paper, we report on the design, fabrication, testing, and modeling of a novel membrane-type polyvinylidene fluoride (PVDF) tactile sensor. The designed assembly consists of a single film of PVDF sensor, which is held between two 12-mm-thick flat Plexiglas plates, each with a 90-mm-diameter center hole. Three rectangular-shaped aluminum electrodes, each 2 mm wide, formed a triangle in the central region of the PVDF film. Using a geometrical mapping process and by applying force at various points on the sensor surface, the loci of the isocharge contours for the three sensing elements are obtained. It is found that the variation in output charge is inversely proportional to the distance from the sensing element and that the exponent for this function is in the range of 0.58–1. Finite element modeling is used to obtain the stress generated in the membrane and to form a basis for the comparison between experimental results and the results of theoretical analysis. There is a good correlation between the theoretical predictions and the experimental data. The designed sensor can be potentially integrated with a medical probe in order to provide tactile mapping.

*Corresponding author, e-mail address: jdargahi@alcor.concordia.ca
**Present affiliation and address: Concordia University, CONCAVE Research Centre, CR-200,
Concordia University, 1445 de Maisonneuve Blvd. West, Montreal, Quebec, Canada H3G 1M8

1.   Introduction

Various kinds of tactile sensors can be used in different biomedical and medical robotics applications to sense a wide range of stimuli, such as, detecting the presence or absence of a grasped tissue/object or even mapping a complete tactile image.[1–3] These sensors normally consist of an array of sensors and, in some cases, might have the capability of measuring a number of tactile properties.[4] In order to define the state of gripping or manipulation of an object or biological tissue, two parameters can convey a significant amount of information, i.e., force and position signatures.[5–8] In this regard, the sensitivity of the tactile sensors strongly depends on several variables, which are mainly determined by the fundamental chemical and physical properties of the sensor. In medical applications, a force sensitivity within the range of 0.1 to 10 N is generally considered satisfactory.[4]

From the biomedical engineering point of view, surgery is a fast developing and is probably the most interesting area of research in which the use of tactile and visual sensing is of critical importance.[9] Despite the fact that minimally invasive surgery (MIS) is only a decade old, it is now being used routinely as one of the most preferred choices for various types of operations.[10] MIS is, in effect, both a visual and tactile procedure, and hence, any reductions in the surgeon's sensory abilities are highly undesirable.[11] Here, in spite of its many advantages (such as, less pain, reduction of trauma, faster recovery time, smaller injuries, and reduction of postoperation complications[9]), MIS reduces the tactile sensory perception of the surgeon during grasping or manipulation of biological tissues. It has been reported that measuring the magnitude and location of the applied forces exerted by the endoscopic grasper during MIS is the fundamental requirement for the safe handling of biological tissues.[12–14] In effect, to perform MIS more efficiently, a surgeon should be able to feel the tissues and detect the presence of blood vessels and ducts during the procedures. This ability is particularly important during controlled manipulation tasks, for example, grasping of internal organs, gentle load transferring during lifting, removing tissues (*e.g.*, gall bladder in laparoscopic surgery and loose bodies in knee arthroscopy), and suturing tissues together.[15] These capabilities coupled with the ability to detect various tactile properties demonstrate the importance of tactile sensing in MIS. Other potential application areas for tactile sensing are rehabilitation procedures, service robotics, agriculture and food processing.[1]

Medical applications of tactile sensing using polyvinylidene fluoride (PVDF) film as a transducer have also been investigated.[8] This work reported on the examination of hardness and softness via palpation. In another study, using a modified commercial endoscopic tool, the magnitude of applied force was measured by strain gauges, and then the position of the grasper was determined with an optical detector.[16] They obtained force-displacement data and identified objects with five different elastic properties. A report has been published on the compliance of hard rubber embedded in a block of foam using remote palpation.[17] Additionally, an endoscopic and robotic micromachined sensor has been designed and fabricated using PVDF film.[14] Design, fabrication, and theoretical studies of a micromachined piezoelectric tactile sensor for an endoscopic grasper have been discussed.[18] The sensor exhibited a high force sensitivity, a high dynamic range, good linearity, and a high signal-to-noise ratio.

Using a pneumatic propulsion method, a microrobot has been designed for colonscopic surgeries.[19] A prototype of an endoscopic tooth-like piezoelectric tactile sensor has been developed to measure both compliance and surface profiles of biological tissues.[20] It consists of a rigid cylinder surrounded by a compliant cylinder. The rigid and the compliant cylinders are fabricated from Plexiglas and an elastomer, respectively. Detailed experimental and finite element analyses of this proposed sensor assembly have also been attempted.[21] Furthermore, a preliminary micromachined version of the same sensor has been successfully built.[22] In another study, a force-moment sensor was placed into the distal shaft of laparoscopic forceps in addition to a tactile sensor array between the jaws of the forceps.[23] The piezoresistive sensor array used was a foil sensor with 64 measuring points. In another study,[24] the pyroelectric effects associated with PVDF-based tactile sensors were distinguished from the piezoelectric effect using different methods. This device has shown an alternative transient approach to distinguish between piezoelectric and pyroelectric signals using only a single PVDF layer of film and hence reducing the complexity of the sensor.

To accomplish the two important goals of determining the magnitude of the applied force and identifying its position, many researchers have attempted to design tactile sensors with a number of discrete sensing elements arranged in matrix form.[25] When applying a force to this matrix, although the force is actually exerted on a single element of the matrix, an undesirable response from the nearest neighbor sensing elements (cross talk) often occurs leading to error in measurement.[26] These problems are often reported where polyvinylidene fluoride (PVDF) film is used to design a matrix of high-spatial-resolution tactile sensors.[27] A further problem with the matrix array of PVDF sensing elements is that, it requires one coaxial cable for each sensing element. The microminiature coaxial cables form a bundle whose size and poor flexibility impose additional limitations. The greater the number of sensing elements, the greater the number of connection points. This, in turn, leads to sensor fragility and causes the design to be a bulky one, which is not appropriate in medical applications. A report has been published on the testing of a piezoelectric membrane tactile sensor, with three sensing elements.[28]

Based on the above facts and requirements, we report on the design and experimental and theoretical analyses of a membrane tactile sensor (MTS) using only three sensing elements. This work is the continuation of a previous report published on this topic.[28] It is shown that the magnitude of the applied force and its position on the surface of the MTS could be obtained using membrane stresses and the triangulation approach with reasonable accuracy and without any cross talk. The designed MTS can be potentially incorporated into a medical probe and be used as a tactile imager. Both finite element modeling and experimental findings are presented and compared with each other.

2.   Materials and Methods

In Section 2.1, the relationship between various physical parameters and the output charge from the PVDF film will be discussed. The various correlations for the off-axis moduli of elasticity are presented in Section 2.2. The implementation of the triangulation approach in locating the coordinates of a point on a two-dimensional plane is explained in

Section 2.3. Finally, Section 2.4 is allocated for discussing the experimental setup and the fabrication of the PVDF sensor.

2.1 *PVDF piezoelectric property*

The beta phase of PVDF forms a crystal symmetry of C_{2v}.[29] For this form of PVDF, the piezoelectric coefficient can be denoted by the following 3×6 matrix.

$$d_{ij} = \begin{bmatrix} 0 & 0 & 0 & 0 & d_{15} & 0 \\ 0 & 0 & 0 & d_{24} & 0 & 0 \\ d_{31} & d_{32} & d_{33} & 0 & 0 & 0 \end{bmatrix}$$

Figure 1 shows the conventional identification of various axes in a PVDF film. The axes utilized are denoted in terms of the drawn direction (direction 1), normal to the drawn direction in the plane of the film (direction 2), and normal to the plane of the film (direction 3). The directions of measurement, i.e., drawn, transverse, or thickness affect the sensitivity of the uniaxially oriented beta form of PVDF. Here, the output charge is directly proportional to the applied tensile force. If the force is exerted in the drawn direction or in the transverse direction, the resulting output charge can be expressed by

$$\frac{Q}{S_e} = d_{3j}\frac{F}{A_j} = d_{3j}\sigma_j \ , \qquad (j=1 \text{ or } 2) \qquad (1)$$
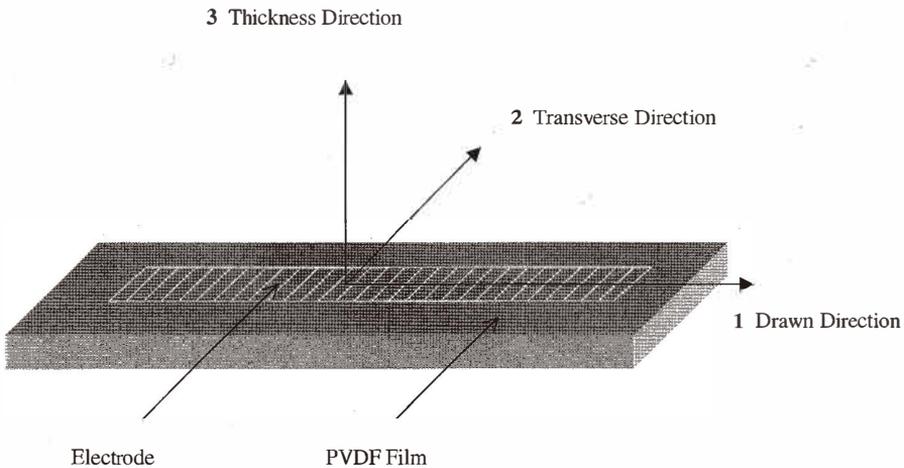

Fig. 1.   Nomenclature of the conventional axes in a PVDF film. The directions 1, 2, and 3, represent the drawn, transverse, and thickness directions, respectively.

where Q is the output charge, S_e is the electrode surface area of the PVDF film, A_1 and A_2 are the cross-sectional areas of the film normal to the direction of the applied force, d_{31} is the piezoelectric strain coefficient in the drawn direction, d_{32} is the piezoelectric strain coefficient in the transverse direction, F is the applied force, σ_1 is the applied tensile stress in the drawn direction, and σ_2 is the applied tensile stress in the transverse direction.

Considering a uniaxially drawn membrane PVDF film on which a point load is applied, the value of the output charge can be expressed by

$$Q = (d_{31}\cos\beta + d_{32}\sin\beta)\ \sigma_r S_e\ , \tag{2}$$

where β is the angle between the drawn direction and the line connecting the position of the applied force with the center of a sensing element, and σ_r is the radial stress in the polymeric membrane.

2.2 Off-axis moduli of PVDF film

The polyvinylidene fluoride film was obtained from Good Fellow Company, USA. The PVDF film used in this study was a uniaxial material and anisotropic. In order to calculate the stiffness moduli and Poisson's ratios of the PVDF film, the following eqs. were used:[30]

$$E_c(\beta) = \frac{E_k}{m^4 + \left[\dfrac{E_k}{G_{12}} - 2v_p\right]m^2 n^2 + \dfrac{E_k}{E_j}n^4} ; \begin{cases} if\ c = x \to k = 1, j = 2, p = 12 \\ if\ c = y \to k = 2, j = 1, p = 21 \end{cases} \tag{3}$$

$$G_{xy}(\beta) = \frac{G_{12}}{m^4 + n^4 + 2\left[2\dfrac{G_{12}}{E_1}(1+2v_{12}) + 2\dfrac{G_{12}}{E_2} - 1\right]m^2 n^2} ; \tag{4}$$

$$v_c(\beta) = \frac{v_p\left(m^4 + n^4\right) - \left[1 - \dfrac{E_k}{E_j} - \dfrac{E_k}{G_{12}}\right]m^2 n^2}{m^4 + \left[\dfrac{E_k}{G_{12}} - 2v_p\right]m^2 n^2 + \dfrac{E_k}{E_j}n^4} ; \begin{cases} if\ c = xy \to k = 1,\ j = 2,\ p = 12 \\ if\ c = yx \to k = 2,\ j = 1,\ p = 21 \end{cases} \tag{5}$$

Here, E_k and E_j are the Young's moduli of elasticity, G_{12}, is the shear modulus of elasticity, and v_c is the Poisson's ratio. $E_c(\beta)$, $G_{xy}(\beta)$, and $v_c(\beta)$ are all functions of β. In the above eqs., $m = \cos\beta$ and $v = \sin\beta$, where β is defined in eq. (2). Table 1 summarizes the values of various constants used in the above eqs.

Based on the data presented in Table 1 and using eq. (3), the variation of the Young's modulus of elasticity in the x and y directions versus the angle of β is plotted in Fig. 2.

Table 1
Summary of the constants used in the off-axis moduli calculations.

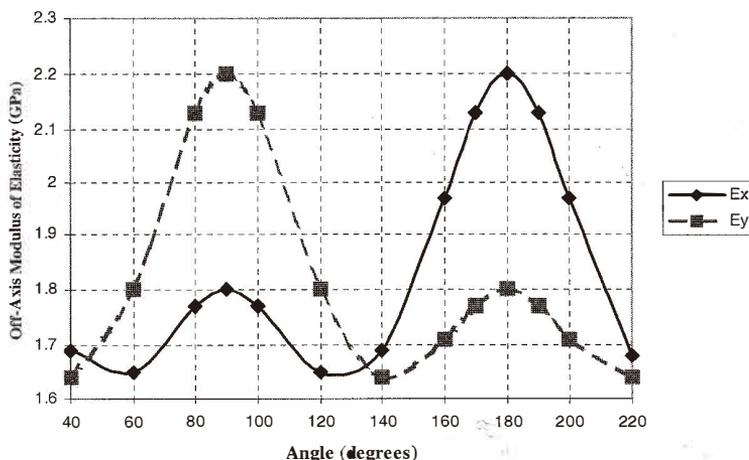| Young's Modulus of Elasticity (GPa)		Shear Modulus of Elasticity (GPa)	Poisson's Ratio	
E_1	E_2	G_{12}	v_{12}	v_{21}
2.20	1.80	0.58	0.35	0.28

Fig. 2.   Variation of the two off-axis moduli of elasticity (E_x and E_y) versus angle.

2.3 *Concept of triangulation*

There are two methods of identifying the location of a particular point on a two-dimensional plane. The first method is the direct reporting of the coordinates of the point (if known). The second method, which is basically an indirect approach, is to identify the distance of the particular point from three reference points whose coordinates are known. In practice, we search for the coordinates of the point, *e.g.*, the location of the application of a force. Therefore, the latter method (called the triangulation approach) is adopted in locating the position of the applied force.

Applying a point force on a membrane-type PVDF film generates stresses in the polymeric sensor. These stresses are related to the output charges detected and as shown in eq. (2), can be used to define the distance from the three sensing elements on the surface of the membrane sensor.

2.4 *Sensor fabrication and experimental setup*

A uniaxially drawn (4:1 ratio) and unpoled film of PVDF was cut to a diameter of 100 mm. The thickness of the resulting circular membrane was 25 μm. Three rectangular-

shaped aluminum electrodes of 2 mm width were deposited by the vacuum deposition method, using masking plates on either side of the PVDF film. The arrangements of the electrodes were so that the intersection of two electrodes (one on either side of the membrane) formed a square sensor element. With this arrangement, the resulting three elements constituted a triangle in the center of the PVDF membrane. Afterwards, the film was poled and tested for its piezoelectric coefficients.

The next step was to perform the mapping process. This was accomplished in two different directions, i.e., radial and angular. Figure 3 demonstrates this concept schematically. In this process, the angular region at each sensing element was divided into subdivisions of 10° and straight lines were drawn passing through the center of each sensing element. Therefore, maps containing concentric circles with rays emanating from their common centers were generated at each vertex of the triangle.

Following the mapping process, the mapped PVDF film was securely held between two 12-mm-thick flat Plexiglas plates, each with a 90-mm-diameter center hole. The detailed construction of the system is presented in Figure 4.

In order to evaluate the performance of the tactile sensor, the experimental setup shown in Figure 5 was utilized. An oscillatory force with a peak of 1 N was applied using a 2-mm-diameter circular probe. The probe was driven by a sinusoidal signal of 15 Hz. A charge amplifier (D.J. Birchal model 04) was used to amplify the charge generated on the surface of the PVDF film. The output charge was recorded on a chart recorder. An oscilloscope was utilized to measure the output signals. A force transducer (Bruel & Kjaer model 820) inserted between the probe and vibration unit measured the applied force magnitude.

One of the parameters that form the basis of comparison between the theoretical analysis and the experimental results is the angle of deflection of the PVDF membrane (α), under loading conditions. Hence, in order to measure this parameter, a clock gauge was
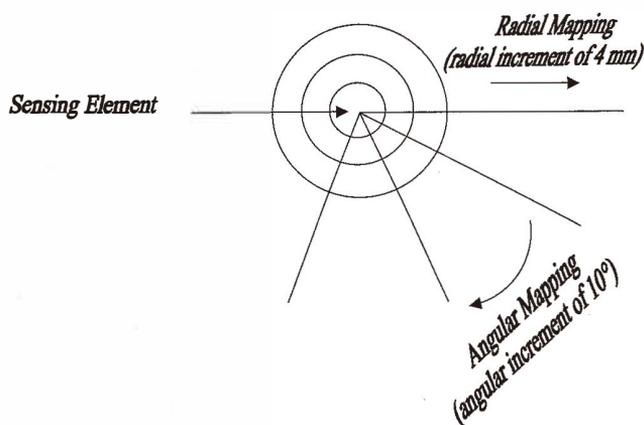

Fig. 3. Schematic representation of the geometric mapping process performed on the surface of the PVDF film.
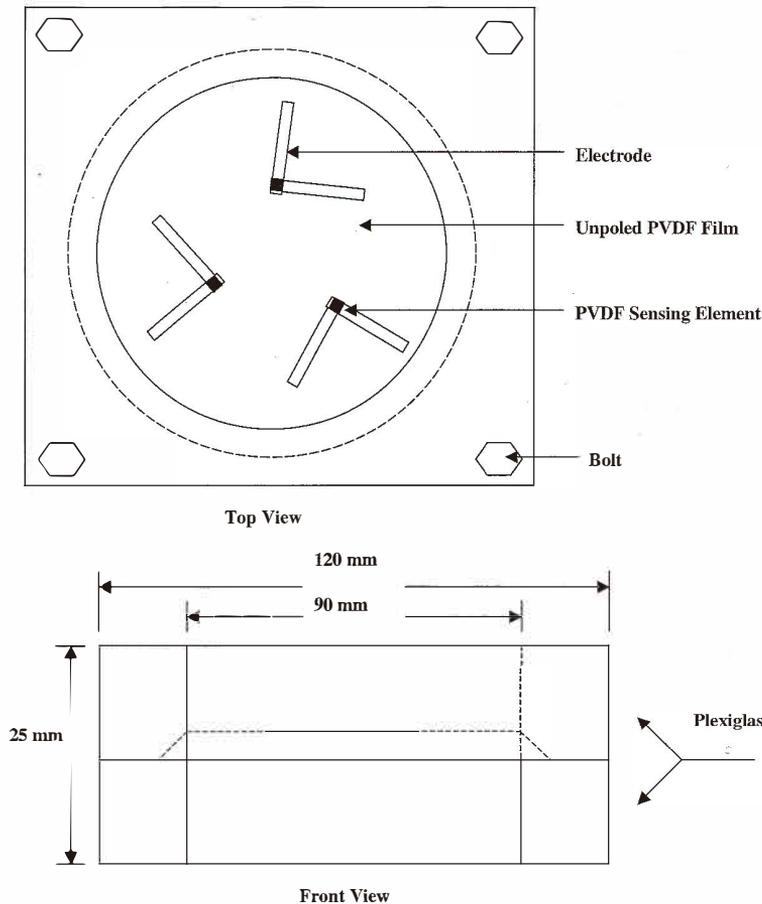
Top View

Front View

Fig. 4.   Construction drawing of the details of the parts used in supporting the PVDF film laterally. The sensing elements are shown by the dark section of the two overlapping electrodes, each on either side of the film.

positioned below the membrane at the probe site. The value of α was calculated based on averaging its value over different experimental runs. α was found to be approximately 15°. This translated into a vertical deflection of approximately 12 mm.

3.   Results

By applying a force in the triangular region shown in Figure 6, the value of output charge was detected by each of the sensing elements (i.e., A, B, and C). The location of the applied force was varied so that the loci of isocharge contours could be obtained. The point of the intersection of isocharge contours is also demonstrated in Fig. 6. This point
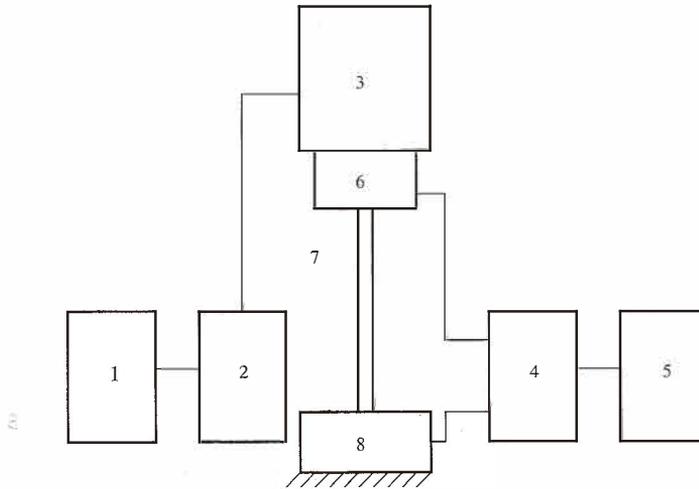
Fig. 5.   Experimental apparatus utilized in applying the dynamic load and measuring the output charge. 1. Power Amplifier 2. Signal Generator 3. Bruel & Kjaer Vibration Unit 4. Charge Amplifier 5. Oscilloscope 6. Force Transducer 7. Probe 8.Tactile Sensor
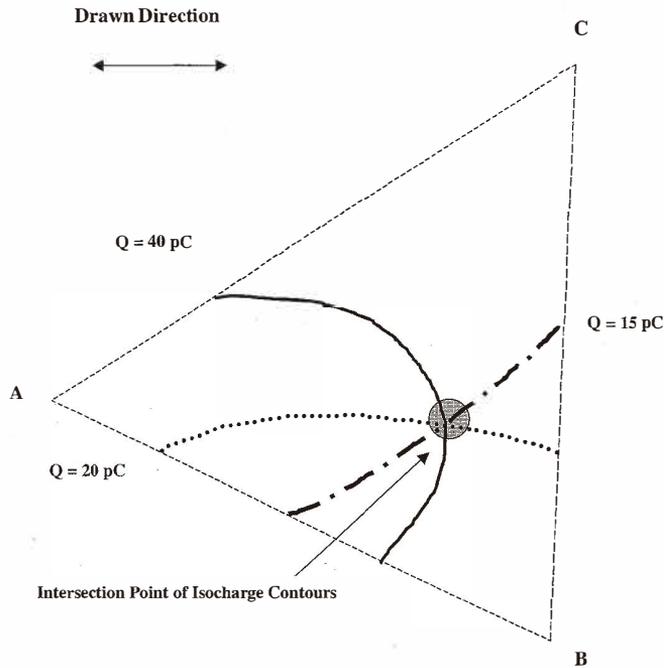

Fig. 6.   Typical isocharge contours obtained by the mapping process. The three isocharge contours of 40 pC, 20 pC, and 15 pC intersect at a point which corresponds to the position of the probe on the sensor surface.

corresponds to an output charge reading of 20 pC for sensing element B, 40 pC for sensing element A, and 15 pC for sensing element C.

The experimental results for sensing element of B are shown in Fig. 7. It can be observed that the output charge from this sensing element drops rapidly as the location of the applied force moves away from the center of the sensing element. For all values of angles from the drawn direction and based on the best fit curves, the trend of this decline follows roughly the equation of the type presented below.

$$Q = C_1(\beta) \cdot d^{C_2} \tag{6}$$

Here, $C_1(\beta)$ is a variable which depends on the value of β, d is the distance from the center of the sensing element, C_2 is the exponent (range of 0.58–1.00), and Q is the output charge. Similar results were obtained for the other two sensing elements (i.e., A and C).

Using the approach explained above, the complete contours of the isocharge of all three sensing elements for various positions of the probe were drawn. These results are shown in Figure 8. Each isocharge contour corresponds to a specific and constant output charge. As can be seen in Figure 8, moving away from each sensing element is accompanied by a reduction in the output charge. For example, in the case of sensing element C, the contours of isocharge drop from 50 pC to 10 pC, as one moves from the vicinity of C to the vicinity of B. It should be pointed out that the contours cover the whole plane of the membrane surface, however, only the parts in the triangular region are shown. Once the map demonstrated in Figure 8 is obtained, the location and the magnitude of the applied force can be determined accordingly, whether or not the force is located in the triangular region.
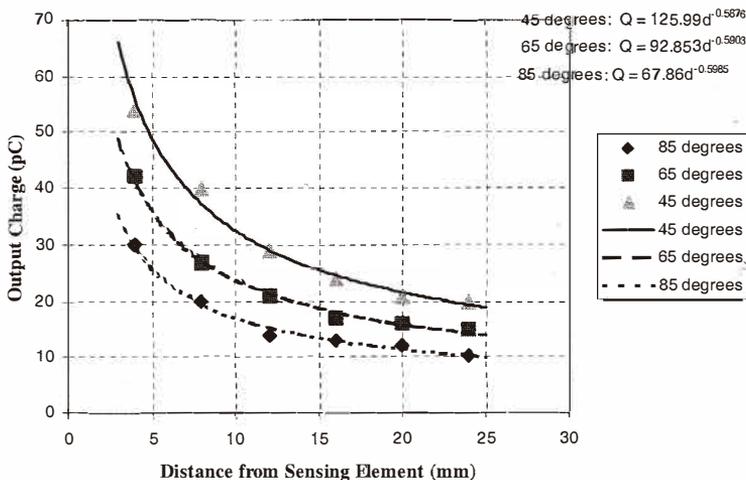

Fig. 7.   Experimental data (discrete data points) showing the variation of the output charge versus the distance from the sensing element of B. The continuous curves are the results of regression analysis.
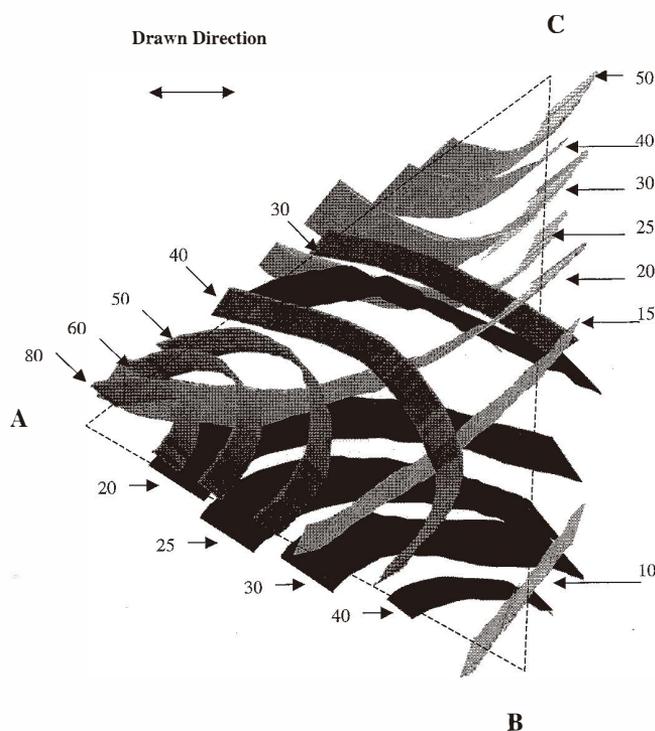
Fig. 8.   Three-dimensional map of the isocharge contours for the PVDF tactile sensor. The charge associated with each isocharge contour is measured in picocoulombs.

    Finite element analysis (ANSYS Package, version 7.0) was used to investigate the theoretical deformation and stress distribution of the designed tactile sensor. This method has been employed successfully in the modeling of various biomedical engineering systems.[31–34] The main purpose of the mathematical analysis was to examine how the PVDF film would behave theoretically under the applied loading conditions. Also, the mathematical analysis was used to make a comparison between the experimental data obtained from the designed tactile sensor and those of theoretical modeling. Figure 9 shows the generated mesh for the PVDF film. The total number of elements was 1374 and the type of elements used was SHELL63. For a typical force with a magnitude of 1 N applied in the vicinity of the center of the film, Fig. 10 illustrates the vertical (z-direction) deflection contours predicted by FEM. As expected, the largest deformations were observed in the region where the force was located. In Figure 11, the deformation profile of the film is plotted versus the radial distance, across the diameter of the structure. Here, the point with a radial distance of 45 mm corresponds to the center of the membrane sensor. The deflection of the membrane is at its maximum at the location of the applied force and has a value of 19.5 mm. On the perimeter of the structure, the deflection is zero.
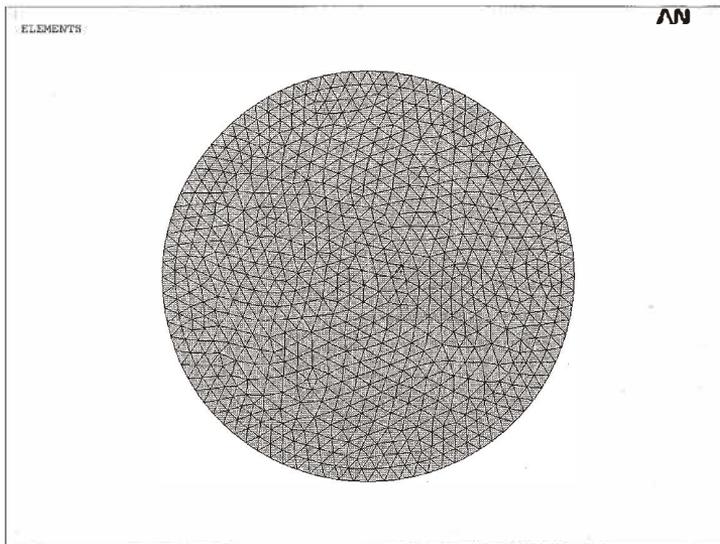
Fig. 9.   Mesh generated in ANSYS for the PVDF circular membrane.
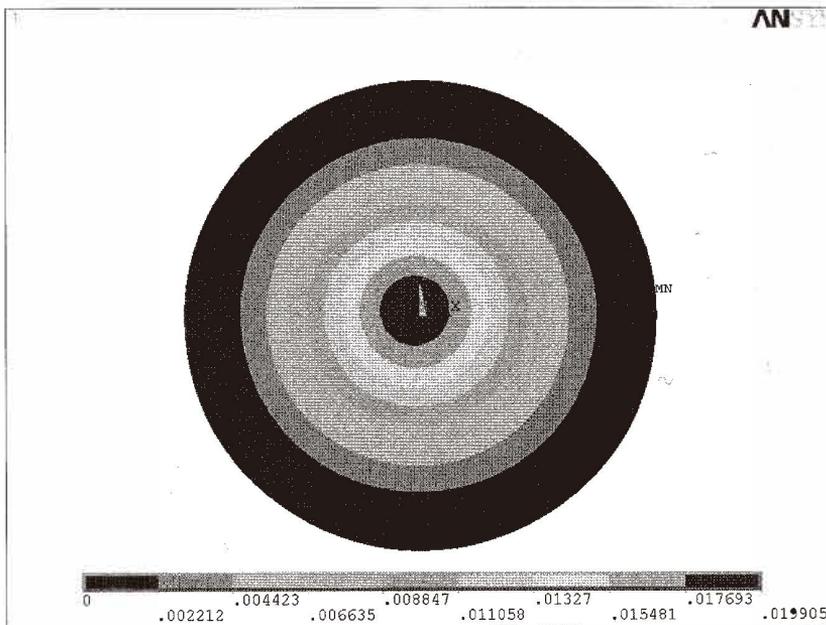

Fig. 10. Deflection contours in the perpendicular direction when a 1-N force is applied in the z-direction.
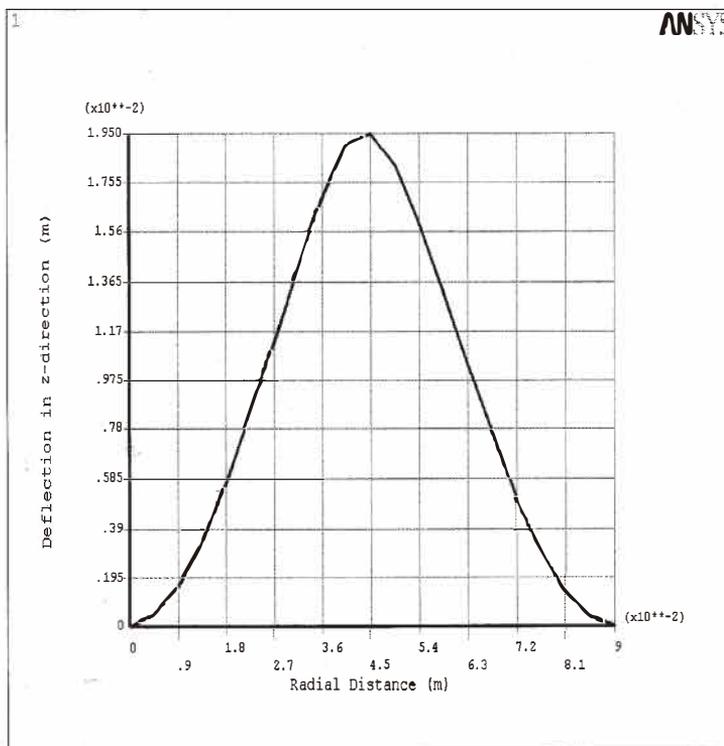
Fig. 11. Variation of vertical deformation of the circular PVDF film across the membrane diameter.

Using the mapping process presented in Figure 3 (this time implementing it in the FEM method), the radial stresses were calculated. For each run, the values of β, and hence, the various moduli were different. These moduli were calculated for each line passing through the center of the sensing elements, using eqs. (3), (4), and (5). The measured values of d_{31} and d_{32} were 6.5 pC/N and 0.65 pC/N, respectively, which were lower than those reported by the manufacturer (i.e., 18 and 2 pC/N, respectively). Figure 12 shows the finite element simulation results of the output charge for three typical angles of 45°, 65°, and 85° versus the distance from the sensing element of B. The results for other angles follow the same general trend. There is a reasonable correspondence between the finite element modeling results and the experimental data (depicted as discrete points in Fig. 12). An average difference of 18% was observed.

4.   Discussion

The experimental errors in the measurement of the isocharge contours came primarily from the position of the center of the probe on the marked points on the membrane surface.
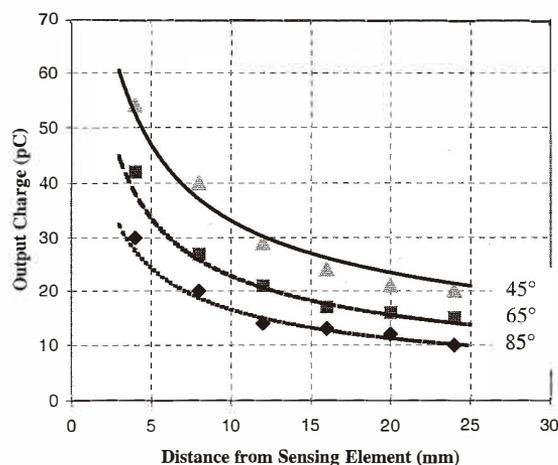
Fig. 12. Comparison between the experimental output charges and the results obtained from finite element modeling.

Thus, a mispositioning of approximately 0.5 mm was estimated, when taking into account the diameter of the circular probe. A maximum error of 12% was expected to have been introduced via this mispositioning. Additionally, in extracting the peak values of the sinusoidal trace from the chart recorder, a 1 mm variation was estimated. This, in turn, introduced an additional error of 5%.

The poling process of the PVDF film was carried out at 100°C with an applied voltage of 2 kV. While applying the voltage, the film was placed on a wooden substrate without any mechanical constraints and held at 100°C for 1 h, then allowed to cool to room temperature (25°C) before the applied voltage was removed. In this process, no attempts were made to optimize the poling conditions, temperature, and voltage. Instead, the focus was on testing the performance of the designed sensor as well as its modeling. The optimization of the poling process is the subject of another research work currently underway in our lab.

If the PVDF film is considered to be a loaded thin circular membrane of radius R and thickness h, which is made of a linear material with Young's modulus E and has Poisson's ratio v, then the applied load P would be related to the maximum deflection $U_{z,max}$ in the following manner.[35]

$$P = \frac{4.E.h}{R(1-v)} \left[\frac{3-v}{4} \left(\frac{U_{z,max}}{R} \right)^3 \right] \tag{7}$$

Using the above analytical equation, with $E \approx 2$ GPa, $R = 45$ mm, $v \approx 0.30$, $P \approx 3 \times 10^5$ Pa, we obtain, $U_{z,max} = 18.5$ mm. This value is in good agreement with the value obtained by

FEM (i.e., 19.5 mm) under similar conditions.

When a compressive force was applied on the surface of the membrane, the deformed shape resembled a cone. As expected, the stresses which developed because of the applied force, were predominantly in the radial direction, and the circumferential stresses were calculated to be negligible. This was mainly due to the fact that little or no expansion was detected in the circumferential direction.

The mapped data shown in Fig. 8, in effect, cover the whole surface of the circular PVDF film. That is to say, regardless of the location of the applied force, we have a map on which the coordinates of every point on the surface are related to the output charges of the three sensing elements. This experimental map can be readily stored on a PC. In practice, when a point force is applied on the sensor, the resulting charges are detected by sensing elements A, B, and C. Then, a comparison is made between the mapped database and the case at hand. The final outputs of this process are the magnitude of the applied force along with its location.

Using the membrane tactile sensing system demonstrated in this research work, it has been shown that by utilizing a flexible substrate (i.e., the PVDF film), the entire polymer surface can be used to sense a force and its position. This was achieved by employing only three sensing elements. As can be observed in Fig. 8, due to the infinite number of isocharge contours which can be drawn and unlike most other tactile sensors, the entire surface of the sensor can be used as an active area of sensing. In other words, the regions which are not active piezoelectrically (since they do not have any electrodes), have been made mechanically active. This is because these mechanically active regions can now transmit stresses to the sensing elements. Therefore, in contrast to matrix tactile sensors where the areas between adjacent sensing elements are inactive, the designed sensor is practically active at all its surface points.

The designed tactile sensor has various immediate applications in biomedical and medical robotics areas. Among these applications are minimally invasive surgeries using endoscopic tools, medical robotics telesurgery procedures (via teletaction[36]), prosthetic fingertips for grasping tissues or objects, and tactile imagers. In the area of tactile imaging, it has been reported that lesions with sizes less than 8 mm in diameter are not palpable by human touch.[37] When touching lesions, just as an electronic camera digitizes the sense of sight, a properly designed tactile imager can digitize the sense of touch. Because lesions are harder than surrounding tissues, for example, breast carcinomas have a modulus of elasticity 5 to 20 times greater than that of surrounding normal tissues, a tactile imager can produce a tactile image corresponding to the size and shape of the lesion.[37] Consequently, the designed PVDF tactile sensor can be incorporated into a medical probe and be used as a tactile imager. In the suggested MTS (membrane tactile sensor) probe, the operator will be able to observe the magnitude of the applied force along with the position of the applied force (on a r-θ coordinate system). The location of the exerted force can appear as dots on the force location chart of the MTS probe.

In order to obtain more details regarding the shape and size of an object which comes into contact with a membrane surface, work is under way in our laboratory using various probe shapes and different supports for the PVDF film. In that work, the focus will be such topics as the boundary recognition of objects.

Acknowledgements

References

1   M. H. Lee and H. R. Nicholls: Mechateronic **9** (1999) 1.
2   J. Dargahi: CSME International Conference 2001 (CSME, Montreal, 2001) p. 21.
3   J. Dargahi: Sensor and Actuators A-Physical **71** (1998) 89.
4   A. Fisch, C. Mavroidis, J. M. Huber and Y. B. Cohen: Haptic Devices for Virtual Reality, Telepresence, and Human-Assistive Robotics, Biologically-Inspired Intelligent Robots, ed. Y. B. Cohen and C. Breazeal (SPIE Press, Bellingham, 2003) p.5.
5   B. Gray and R. S. Fearing: International Conference on Robotics and Automation 1996 (IEEE, Minneapolis, 1996) p. 1.
6   J. Dargahi and S. Payandeh: International Conference on Sensor Fusion: Architectures, Algorithms and Applications 1998 (SPIE, Orlando, 1998) p. 122.
7   J. Dargahi, M. Normandeau, J. Milne, M. Parameswaran and S. Payandeh: International Conference on Sensor Fusion: Architecture, Algorithms and Applications 2000 (SPIE, Orlando, 2000) p. 349.
8   P. Dario: Sensors and Actuators A-Physical **26** (1991) 251.
9   I. Brouwer, J. Ustin, L. Bentley, A. Sherman, N. Dhruv and F. Tendick: Medicine Meets Virtual Reality **81** (2001) 69.
10   H. H. Rininsland: Endoscopic Surgery and Allied Technologies **1** (1993) 154.
11   B. Hannaford, J. Trujillo, M. Sinanan, M. Moreyra, J. Rosen, J. Brown, R. Leuschke and M. MacFarlane: Medicine Meets Virtual Reality **50** (1998) 265.
12   E. Crago, J. Nakai and H. J. Chizeck: IEEE Transactions on Biomedical Engineering **38** (1991) 17.
13   J. Dargahi, A. Eastwood and I.J. Kemp: International Conference on Sensor Fusion: Architectures, Algorithms and Applications 1997 (SPIE, Orlando, 1997) p. 20.
14   J. Dargahi, S. Payandeh and M. Parameswaran: International Conference on Robotics and Automation 1999 (IEEE, Detroit, 1999) p. 299.
15   H. H. Melzer, M.O. Schurr, W. Kunert, G. Buess, U. Voges and J. U. Meyer: Endoscopic Surgery and Allied Technologies **1** (1993) 165.
16   A. Bicchi, G. Canepa, D. De Rossi, P. Iacconi and E. P. Scilingo: International Conference on Robotics and Automation 1996 (IEEE, Minneapolis, 1996) p. 884.
17   R. D. Howe, W. J. Peine, D.A. Kontarinis and J. S. Son: IEEE Engineering in Medicine and Biology Magazine **14** (1994) 318.
18   J. Dargahi, M. Parameswaran and S. Payandeh: Journal of Microelectromechanical Systems **9** (2000) 329.
19   P. Dario, M. C. Carrozza, L. Lencioni, B. Magnani and S. D'Attanasio: International Conference on Robotics and Automation 1997 (IEEE, Albuquerque,1997) p. 1567.
20   J. Dargahi: Journal of Mechanical Design **124** (2002) 576.
21   H. Singh, J. Dargahi and R. Sedaghati: 2nd International Conference on Sensors 2003 (IEEE, Toronto, 2003) Accepted for Publication.

22   N. P. Rao, J. Dargahi, M. Kahrizi and S. Prasad: Canadian Conference on Electrical and Computer Engineering 2003 (CCECE, Montreal, 2003).

23   H. Fischer, B. Neisius and R. Trapp: Tactile feedback for endoscopic surgery, Interactive Technology and a New Paradigm for Health Care, eds. K. Morgan, M. Satava, B. Sieburg, R. Mattheus, and J.P. Christensen (IOS Press, Amsterdam,1995) p. 114.

24   J. Dargahi: CSME International Conference 2001 (CSME, Montreal, 2001) p 21.

25   R. R. Reston and E. S. Kolesar: National Aerospace and Electronics Conference 1990 (IEEE, Daton, 1990) p. 1139.

26   E. S. Kolesar, P. R. Reston, D. G. Ford and R. C. Fitch: Journal of Robotic Systems **9** (1992) 37.

27   P. Dario and G. Buttazzo: International Journal of Robotics Research, **6** (1987) 24.

28   J. Dargahi: Sensors and Actuators A-Physical **80** (2000) 23.

29   J. Dargahi: The application of polyvinylidene fluoride as a robotic tactile sensor, Ph.D. Dissertation, Glasgow Caledonian University, Glasgow, Scotland, (1993).

30   D. Gay: MatÈriaux Composites (Hermes Publishing Company, Paris, 1997) Chapter 2.

31   J. Dargahi, S. Najarian and S. Amiri: Journal of Bio-Medical Materials and Engineering, Accepted for Publication, To appear in issue **14** (2004).

32   S. Najarian and B. Heidari: European Society of Biomechanics Conference 2000 (ESBC, Dublin, 2000) p. 207.

33   S. Najarian and H. Sharifzadeh: Biomedical Sciences Instrumentation **38** (2001) 337.

34   S. Najarian and A. Pashaee: Biomedical Sciences Instrumentation **38** (2001) 185.

35   G.W. Brodland and H. Cohen: ASME Journal of Applied Mechanics, **54** (1987) 287.

36   R.S. Fearing, G. Moy and E. Tan: International Conference on Robotics and Automation 1997 (IEEE, Albuquerque, 1997) p. 3093.

37   T. A. Krouskop, T. M. Wheeler, F. Kallel, B. S. Garra and T. Hall: Ultrasonic Imaging **20** (1998) 260.